Insect Biochemistry and Molecular Biology 115 (2019) 103246

Contents lists available at ScienceDirect

Insect Biochemistry and Molecular Biology

journal homepage: www.elsevier.com/locate/ibmb

Mutations in *Nl*InR1 affect normal growth and lifespan in the brown planthopper *Nilaparvata lugens*

Yu Zhao, Gang Huang, Wenqing Zhang*

State Key Laboratory of Biocontrol and School of Life Sciences, Sun Yat-sen University, Guangzhou, 510275, China

ARTICLE INFO

Keywords:
Insulin/IGF signaling (IIS)
*Nl*InR1
Growth
CRISPR/Cas9
Brown planthopper (BPH)

ABSTRACT

The brown planthopper (BPH) *Nilaparvata lugens* contains two insulin receptor homologues, designated *Nl*InR1 and *Nl*InR2. *Nl*InR1 is strikingly homologous to the typical InR in insects and vertebrates, containing a ligand-activated intracellular tyrosine kinase catalytic domain. Herein, we report an optimized CRISPR/Cas9 system to induce mutations in the *Nl*InR1 locus in BPH, consisting of a Cas9 plasmid that is specifically expressed in the germline via the *Nl*vasa promoter and versatile sgRNA expression plasmids under the control of the U6 promoter. We systematically evaluated the efficiency of injection mix compositions and demonstrated an appropriate combination of Cas9/sgRNA to target essential genes. Furthermore, we showed that homozygous mutants for the *Nl*InR1 gene are early embryonic lethal, whereas heterozygous mutants grow more slowly, exhibit a severe reduction in body weight and wing size and live longer than the wild type. Interestingly, the severity of the mutant phenotype was different when targeting distinct important domains of the *Nl*InR1 locus. The severity of the mutant phenotype is similar to that of insulin/insulin-like growth factor (IGF) signaling pathway deficiencies in vertebrates, suggesting a conserved function of *Nl*InR1 in the regulation of development and longevity. Global expression profiling suggests that *Nl*InR1 regulates many cellular processes in BPH, including insulin resistance, phototransduction, metabolism, endocytosis, longevity, biosynthesis and protein processing. Our results also pave the way for understanding the precise molecular mechanism of insulin signaling in wing polyphenism in insects.

1. Introduction

The insulin/IGF signaling pathway plays essential roles in growth, development and metabolism in metazoans. The biological action of this pathway is mediated by a transmembrane receptor, called insulin/IGF receptor, which belongs to a large family of receptor tyrosine kinases (RTKs) and has features in common with other RTKs in signal transduction. Insulin receptors are widely distributed on the surface of animal cells where its function in cellular metabolism and growth is well known (Saltiel and Kahn, 2001). Insulin receptors comprise two α and two β subunits. The α subunit of the protein is entirely on the outside of the cell and contains the insulin-binding site. Insulin binding induces structural changes of the α subunit leading to tyrosine autophosphorylation of the β subunit, with subsequent activation of tyrosine kinase activity of insulin receptor, eventually initiating downstream signaling processes (Belfiore et al., 2009). In the fruit fly *Drosophila melanogaster*, the homologue of the insulin/IGF receptor (InR) is required for normal growth, germline stem cell (GSC) maintenance and life span regulation (Hsu and Drummond-Barbosa, 2009; Oldham and Hafen, 2003). InR homozygous mutants lead to embryonic lethality (Fernandez et al., 1995), only flies with heteroallelic combinations of InR mutations result in viable, dwarf adults with developmental delay, female sterility, reduced organ and body size (Brogiolo et al., 2001; Tatar et al., 2001). In the nematode *Caenorhabditis elegans*, DAF-2 (worm insulin receptor orthologue) mutants are smaller because of fewer and smaller cells and live longer than wild type (WT) (Kenyon et al., 1993). In the house mouse *Mus musculus*, insulin-like growth factor type 1 receptor (IGF-1R) is homologous to insulin receptors. IGF-$1R^{+/-}$ mice live on average 26% longer than their WT littermates, null mutants are not viable (Holzenberger et al., 2003). Genetic studies have shown that the InR signaling pathway is evolutionarily conserved in metazoans, including ligand-induced structural changes within the receptor dimer, leading to autophosphorylation of tyrosine residues, allowing recruitment and phosphorylation of specific substrate adaptor proteins (White, 1998). Subsequent activation of downstream signaling molecules, such as phosphoinositide 3-kinase (PI3K), Grb2, Nck, Syp, and Shc (Soldatos et al., 2003; Vanhaesebroeck et al., 2001), activate several other kinase signaling pathways, most notably Protein kinase B

* Corresponding author.
E-mail address: lsszwq@mail.sysu.edu.cn (W. Zhang).

https://doi.org/10.1016/j.ibmb.2019.103246
Received 1 August 2019; Received in revised form 7 October 2019; Accepted 8 October 2019
Available online 13 October 2019
0965-1748/

(PKB, also known as Akt) and MAPK (Taniguchi et al., 2006). Different activated signaling molecules eventually lead to distinct downstream processes via diverse protein targets and different expression levels of the insulin receptor may regulate signaling in a tissue-specific pattern.

In the brown planthopper (BPH) *Nilaparvata lugens*, *Nl*InR1 and *Nl*InR2 are highly homologous to *Drosophila* InR. Both genetic and biochemical analyses suggest that *Nl*InR1 shows greater similarity to the canonical InR (Lin et al., 2018; Zhang et al., 2019). It has been reported that *Nl*InR1 and *Nl*InR2 mediate opposite effects on wing morph determination via RNA interference (RNAi) (Xu et al., 2015). Nymphal knockdown of *Nl*InR1 results in a strong bias towards short-winged adults with normal wing veins, indicating that *Nl*InR1 constrains its functions to modulate wing size rather than the developmental pattern. *Nl*InR1 is widely expressed in most tissues and developmental stages, indicating the broad influence of this signaling pathway. However, the systemic effect on growth and metabolism, biological roles in the normal physiology of *Nl*InR1 are generally not well understood. In addition, the identities of specific gene targets of *Nl*InR1 that participate in regulation remain unclear.

Although RNAi can be useful in BPH in certain circumstances, it is important to note that this approach induces phenotypic changes that are complicated to interpret due to incomplete gene knockdown. Thus, some residual activity of the target gene remains in dsRNA-treated animals throughout the experimental period. Gene knockout is undoubtedly the best way to compare the phenotypes of different mutations of a target gene, allowing us to conclusively test the role of certain genes or genetic pathways. Functional genetic tools, such as transposon mutagenesis (e.g., P element, Hermes, Mos1, Minos, and piggyBac) or targeted mutagenesis (e.g., TALENs, ZFNs, and CRISPR/Cas9), have not been widely available in BPH; only one mutational analysis using CRISPR/Cas9 to create null mutants of the eye pigmentation gene has been reported to date (Xue et al., 2018). We speculate that the complex life cycle and unoptimized conditions during the *in vitro* culture of BPH embryos have impeded successful application of these genetic engineering technologies.

To explore the pleiotropic functions of *Nl*InR1 in the insulin signaling pathway, we have undertaken a reverse genetics approach by using CRISPR/Cas9 mutagenesis to isolate mutant alleles in the *Nl*InR1 locus. We developed an optimized CRISPR/Cas9 tool to knock out essential genes consisting of a set of systematically evaluated combinations of Cas9 and sgRNA sources. The effects on the rate of mutagenesis of sgRNA expressed by different promoters from U6 snRNA genes and germline-restricted expression of Cas9 plasmid were also first evaluated. An appropriate combination of Cas9 and sgRNA expression plasmid in our study allowed the targeting of essential genes with transmission rates above 30% with ideal G_0 survival rates. The biological importance of the InR in higher organisms and the continuous expression of *Nl*InR1 mRNA during BPH development suggested that *Nl*InR1 activity would be crucial for survival. Therefore, *Nl*InR1 mutant lines were identified initially using heterozygous mutations. Subsequently, screening was performed to identify homozygous mutant lines. Finally, our data not only confirmed deeply conserved roles for *Nl*InR1 in growth and development similar to those of the IGF-I receptor in vertebrates but also revealed that *Nl*InR1 is a haploinsufficient gene in BPH.

2. Materials and methods

2.1. Insects

The BPHs used in this study were originally obtained from Guangdong Academy of Agricultural Sciences (GAAS), reared on susceptible fresh rice seedlings of Huang Huazhan (bought from GAAS, Guangzhou, Guangdong, China) in a greenhouse at 26 ± 0.5 °C with 80 ± 10% relative humidity under a photoperiod of L16: D8 h.

2.2. CRISPR reagent preparation

We designed short guide RNA (sgRNA) by searching sequences corresponding to 5′-GGN18NGG-3′ or 5′-N20NGG-3′ in the *Nl*InR1 (KF974333.1) exon regions on both DNA strands using two websites: ZiFiT (http://zifit.partners.org/ZiFiT) and ChopChop (http://chopchop.cbu.uib.no/). We then tested for homologous sites by local BLAST searches against the BPH genome and transcriptome databases to minimize potential off-target binding, sgRNAs with lowest off-target scores were selected. Because the T7 promoter requires a dinucleotide GG at the transcription initiation site, a GG dinucleotide was added to the 5′ end of target sites that lack this feature. The extra nucleotides mismatched at the 5′ end of the sgRNA do not affect sgRNA function (Fu et al., 2014). Target sequences that did not contain polymorphisms were used.

sgRNAs were *in vitro* transcribed from PCR amplicons. Briefly, linear DNA templates for specific sgRNAs were amplified from pMD18T-sgRNA plasmid (gift from Yikang S. Rong, Sun Yat-sen University) with a forward primer encoding the T7 polymerase-binding site and the sgRNA target sequence and a common reverse primer with Q5 high-quality DNA polymerase (New England Biolabs, Ipswich, Massachusetts, USA). The PCR products were purified using the Wizard SV Gel and PCR Clean-Up Kit (Promega, Fitchburg, WI, USA) and *in vitro* transcription was performed with the T7 RiboMAX™ Express RNAi Kit (Promega, Fitchburg, WI, USA). The sgRNA transcripts were purified with a MEGAclear Transcription Clean-Up Kit (Life Technologies, Carlsbad, California, USA). The recombinant *Streptococcus pyogenes* Cas9 (SpCas9) protein was purchased commercially (Invitrogen, Carlsbad, CA, USA). The locations of target sites and primers for constructing sgRNAs are shown in Fig. 2a and Supplementary Table S1, respectively.

2.3. Generation of Cas9 and sgRNA plasmid

We chose the *Nl*vasa regulatory regions for the expression of Cas9 in BPH germline cells. First, a BPH codon-optimized SpCas9 sequence encoding 3xFLAG-NLS-Cas9-NLS was synthetically produced (IGEbio, Guangzhou, Guangdong, China) and ligated into the EcoRI and XbaI sites of the pUC19 vector to produce pUC19-Cas9. To generate the vasa-Cas9 (MN224142) expression plasmid, we amplified the *Nl*vasa promoter from PEASY-pvasa, the *Nl*vasa 3′ UTR and 3′ flanking region (983 bp) from BPH DNA, the Cas9 coding sequence and the pUC19 plasmid backbone from pUC19-Cas9 (see Supplementary Table S1 for the primers). The final plasmid was assembled with four segments by Gibson assembly according to the manufacturer's protocol (New England Biolabs, Ipswich, Massachusetts, USA). Unless otherwise noted, all PCR inserts were produced with Phanta Super-Fidelity DNA Polymerase (Vazyme Biotech, Nanjing, Jiangsu, China) and were sequencing verified.

We developed the sgRNA expression vectors with the U6 snRNA pol III promoters. BPH U6 snRNA genes were found in the BPH genome by performing local BLAST searches using the conserved U6 snRNA genes. Three U6 snRNA genes with the same coding regions but highly differentiated flanking sequences were isolated and named U6a (MN224139), U6b (MN224140), and U6c (MN224141). We conservatively used the 431-bp upstream regulatory sequences of U6a to construct U6a-sgRNA, the 447-bp upstream regulatory sequences of U6b to construct U6b-sgRNA and the 455-bp upstream regulatory sequences of U6c to construct U6c-sgRNA. The U6a, U6b, and U6c promoter sequences were amplified by PCR using genomic DNA and assembled into the pBluescript II (SK-) backbone with a heterologous sequence amplified from 3xP3-DsRed2 and a sgRNA scaffold amplified from pMD18T-sgRNA using Gibson assembly. The PCR primers are listed in Table S1. The heterologous sequence between the BbsI sites was used as an indicator of successful ligation of the target sequence. This three-U6 entry vectors allowed the insertion of annealed

complementary oligonucleotides into the BbsI-linearized vector to produce the target-specific sgRNA plasmid. Cloning procedures to introduce target sequence into vectors are described in Supplementary Fig. S5. Oligos for the generation of sgRNA expression plasmids targeting *Nl*InR1 can be found in Table S1.

2.4. Embryo microinjection

Embryonic microinjection was performed as previously described (Lobo et al., 2006) with minor modifications. Briefly, pre-blastoderm BPH embryos were dissected from rice sheaths within 2 h after oviposition (Xue et al., 2018). The collected embryos were transferred using a pair of tweezers (World Precision Instruments, Sarasota, FL, USA) to a strip of filter paper (Whatman, Maidstone, UK) that had been lightly moistened with ddH_2O, oriented in a straight line with the same posterior and ventral side orientation, then transferred onto double-sided tape (3M Scotch, St. Paul, Minnesota, USA) attached to a microscope slide along the long edge by gently pressing the slide onto the dorsal surface of embryos. The embryos were covered with a few drops of halocarbon oil 700 after desiccation in a desiccation chamber containing silica gel-self indicator for approximately 2–4 min. Injections were performed using an Olympus SZX2-ILLT stereomicroscope equipped with a M-152 three-dimensional manual micromanipulator (Narishige, Tokyo, Japan) and an IM-9B microinjector (Narishige, Tokyo, Japan). For the delivery of Cas9 protein/sgRNA ribonucleoprotein complexes (Cas9 RNPs), 200 ng/μL of Cas9 protein, 50 ng/μL of each sgRNA and 0.2% phenol red were coinjected as a mixture. For the delivery of plasmid DNA, the injection solution consisted of 300 ng/μL vasa-Cas9 plasmid, 100 ng/μL of each sgRNA plasmid and 0.2% phenol red. Embryos no older than 3 h were gently pierced into the posterior end with the needle and injected for 1 nL. After injection, embryos were transferred on their microscope slides to a plastic slide box containing a moistened paper towel and placed in a plant growth chamber at 26 °C and 80% relative humidity. Embryos that displayed signs of development at 6–7 days post-injection were removed and transferred to a Kimwipe wipers and rolled gently on the Kimwipe to remove as much mineral oil as possible. Cleaned embryos were placed in rice sheaths until the first-instar nymphs hatched 1–4 days later and were then reared to adulthood under standard BPH rearing conditions. G_0 males and females were outcrossed to WT BPHs and for phenotypic analysis.

2.5. Molecular characterization of mutations

To identify the CRISPR/Cas9-induced mutation, the DNA fragments surrounding the *Nl*InR1 target sites were first amplified by PCR using genomic DNA extracted from individual BPHs by the Insect DNA Kit (Omega, Norcross, GA, USA). PCR amplicons were gel purified and subsequently sequenced. Heterozygous BPHs usually yielded an overlay in the chromatogram from the mutant and WT *Nl*InR1 alleles. To detach detailed indels in *Nl*InR1 mutants, PCR products with double peaks were ligated into the PEASY-Blunt cloning vector (TransGen Biotech, Beijing, China) and at least 10 single colonies were Sanger sequenced. All PCRs were performed using Q5 High-Fidelity 2X Master Mix (New England Biolabs, Ipswich, Massachusetts, USA). The PCR conditions were as follows: 98 °C for 30 s, followed by 35 cycles of 98 °C for 10 s, 55 °C for 20 s and 72 °C for 30 s, and final extension at 72 °C for 2 min. The primers used are listed in Table S1.

2.6. Screening of mutations and image acquisition

To assess germline mutations, all G_0 adult BPHs that developed from injected embryos were outcrossed to WT BPHs. The G_1 offspring were screened for wing morph at the adult stage. All offspring were screened. The overall heritable transmission rates were calculated as the fertile crosses that produced mutant progeny out of the number of total progenies for a given sgRNA target. Mutagenesis events were sequence verified from G_1 adults. Whole-body phenotypes of BPHs were photographed under a Leica DFC 450 C camera equipped with a Leica M205 FA stereomicroscope using the digital imaging system LAS v4.5. The dissected forewings of adult BPHs (0–12 h after eclosion) were imaged using an Axiocam HR3 camera mounted on a Zeiss SteREO Discovery.V20 Macro/Stereo Microscope. All images were processed using Adobe Photoshop CC 2019, adult body length, pronotum width and wing size were then measured using ImageJ (NIH, Bethesda, MD, USA).

2.7. Measurement of BPH weights, duration of nymphal development and lifespan

The average individual mass of the 1-day-old adults of each genotype in the G_1 generation was measured and calculated by weighing BPHs ingroups (6 adults) using a ME204E analytical balance (Mettler Toledo, Columbus, Ohio, USA). The experiment was repeated ten times. BPHs were reared under the same fresh rice plants and were age-matched (0–12 h after eclosion) before weighing. The first instar G_1 nymphs were transferred and reared individually in glass tubes with fresh rice seedlings. The numbers of nymphs developing to the adult stage were recorded daily and subsequently used to analyze the nymphal duration using SPSS (IBM Corporation, Armonk, New York, USA).

Survivorship and age-specific mortality were constructed at 26 ± 0.5 °C with 80 ± 10% humidity and a light-dark cycle of L16: D8 h by the extinct cohort method. For the lifespan analysis of mutant and WT adults, at least 80 adults of mixed-sex from each genotype were reared on fresh rice plants. Rice plants were changed every 3 days, the numbers of dead individuals were counted daily. Three replicate cages with distinct cohorts of insects were concurrently assayed.

2.8. Analyses of female fecundity

To observe fecundity and hatching rate for female BPHs, each newly emerged mutant female adult was paired with two WT male adults. The BPH pairs were reared separately in a plastic cage with fresh rice plants to produce offspring for 5 days. Subsequently, the BPH pairs were transferred onto new fresh rice plants to produce offspring for another 5 days. The eggs in rice plants were maintained for 12 days for counting the number of newly hatched nymphs every day. The number of unhatched eggs was counted under a S9D stereomicroscope (Leica, Wetzlar, Germany) by dissecting the stem of rice plants. Each group included 20 pairs of adults, the experiments were carried out for 3 biological replicates.

2.9. Next-generation sequencing

We used the Illumina HiSeq Xten platform to deep sequence pools of G_0 DNA. Briefly, 6 adult (3 males and 3 females) individuals were used to generate a single sequencing library via a two-step PCR. The first PCR amplified a 250-280-bp DNA fragment extended with small overhangs surrounding the sgRNA target site using primers listed in Table S1. Sample-specific barcodes and Illumina sequencing adapters were tagged by fusion PCR using the VAHTS DNA Adapters set1 Kit (Vazyme Biotech, Nanjing, Jiangsu, China). PCR products were purified using AMPure XP beads. Target amplicons were quantified using a Qubit 4 Fluorometer (Life Technologies, Carlsbad, California, USA) and pooled in an equimolar ratio. The normalized libraries were sequenced with a 2*150-bp paired-end run. Sequencing reads were aligned to the WT *Nl*InR1 genomic sequence and examined for indels using a series of shell scripts and python packages developed previously (Kistler et al., 2015).

2.10. Supplemental experimental procedures

Details of the following methods are provided in supplemental experimental procedures: 5′- and 3′-rapid amplification of cDNA ends

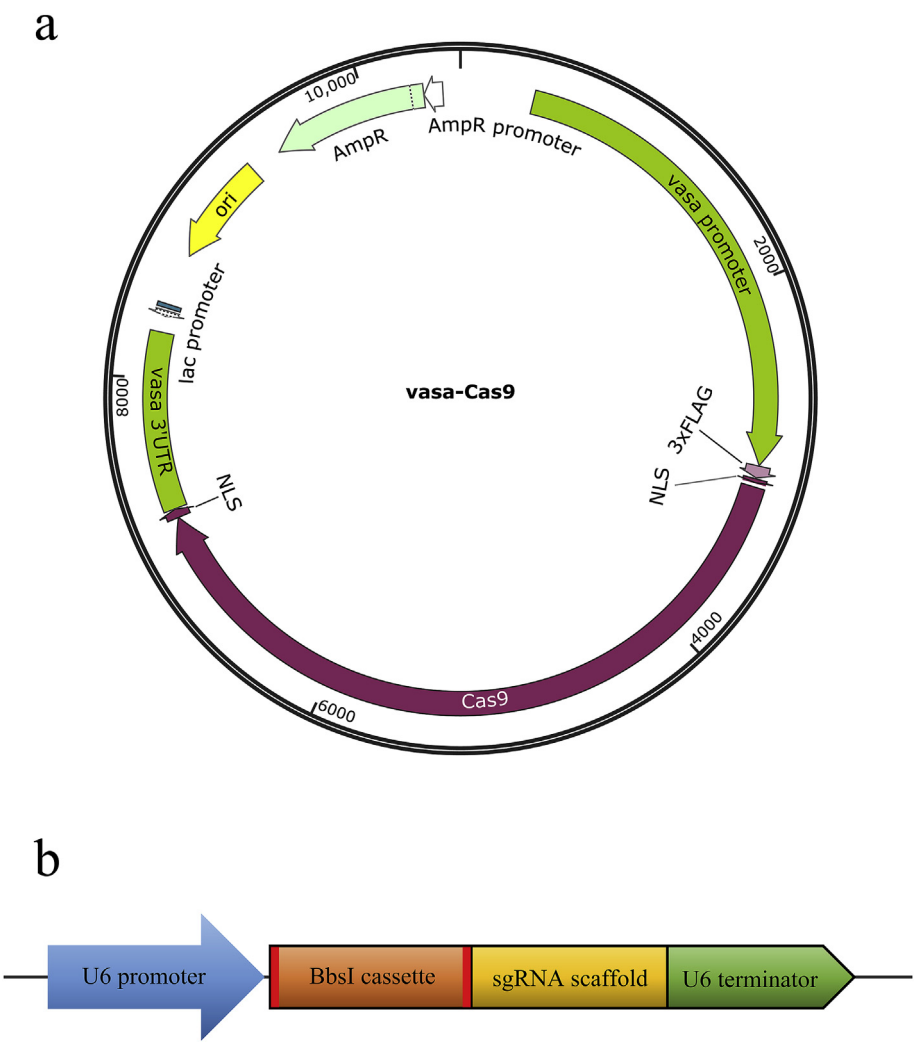

Fig. 1. Optimized vector systems for genome editing with CRISPR/Cas9 in BPH. (a) The vasa-Cas9 plasmid encodes the BPH codon-optimized Cas9 gene under the regulation of the *Nl*vasa promoter and 3′-downstream regulatory region. (b) Schematic of the sgRNA-expressing plasmid used in this study (sgRNA-expressing cassette using three distinct BPH U6 gene promoters, including U6a, U6b and U6c promoter).

(RACE), sequence analysis of *Nl*vasa, luciferase reporter assays, qRT-PCR, RNA-Seq analysis, and Western blotting.

2.11. Statistical analysis

Data are presented as the means ± SEM. All statistical analyses were performed using GraphPad Prism 8 with the levels of statistical significance set at $*P < 0.05$ and $**P < 0.01$. The differences in the means between groups were compared using one-way ANOVA or Student's *t*-test.

3. Results

3.1. Construction of the CRISPR/Cas9 expression plasmids for BPH mutagenesis

A vector system allowing endogenous expression of Cas9 and sgRNA is an alternative form to deliver CRISPR/Cas9 sources that is easy to use and efficient. To express Cas9 in the germline of BPH, we engineered a Cas9 plasmid under the *Nl*vasa promoter (Fig. 1a). We theorized that the *Nl*vasa promoter would restrict the expression of Cas9 in germ cells, which may be helpful for viability due to fewer somatic mutations when targeting essential genes. The putative *Nl*vasa orthologue was identified with a BLAST program using *D. melanogaster* vasa as a query sequence in the BPH genome and transcriptome databases. The candidate sequence with the highest score was confirmed by a reverse BLAST against the NCBI non-redundant protein database. The full-length *Nl*vasa transcript of approximately 2.5 kb in length with a 136-bp 5′ UTR and 144-bp 3′ UTR was obtained through 5′-RACE and 3′-RACE (Supplementary Fig. S1). *Nl*vasa showed high-level sequence conservation to other vasa subfamily proteins in each putative domain according to sequence alignment and the most conserved residues spanning the DEAD-box RNA helicase domains (Supplementary Fig. S2). High-level sequence conservation was also observed in a maximum-likelihood phylogenetic tree using full-length protein sequences (Supplementary Fig. S3). We therefore concluded that MN224138 encodes the full-length protein and it is the *Nl*vasa gene. To characterize the 5′-upstream regulatory region of the *Nl*vasa gene, we cloned different truncated promoter sequences into the pGL3-basic vector, after which we identified the potential cis-elements for promoter activity involved in the regulation of *Nl*vasa transcription (Supplementary Fig. S4a). The *Nl*vasa promoter (-2463, +136) had the highest activity level, suggesting that the -2463 and + 136 region is important for enhancing the transcriptional activity of the *Nl*vasa gene. We inserted this promoter fragment into a plasmid upstream of the codon-optimized SpCas9 gene. Downstream of the coding sequence of SpCas9 we included a 983 bp sequence starting from the stop codon containing the entire 3′ UTR of the *Nl*vasa gene, together forming the vasa-Cas9

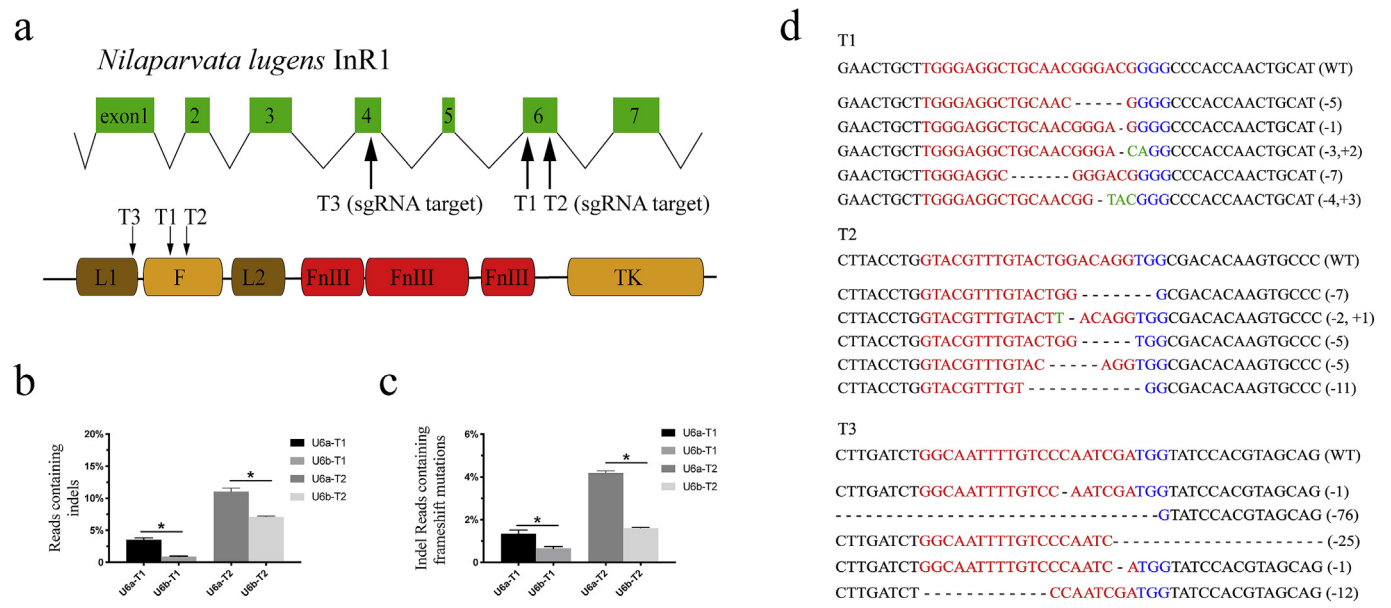

Fig. 2. Quantifying mutagenesis efficiency induced by the CRISPR/Cas9 system. (a) Schematic diagram of three sgRNA target sites designed in the *Nl*InR1 locus. Exons of *Nl*InR1 are shown in green boxes, T3 sgRNA targets the fourth exon, T1 and T2 target the sixth. Corresponding predicted functional domain of the sgRNA-targeted site is shown as coloured blocks. L, leucine-rich repeat domain; F, furin-like repeats; FnIII, fibronectin type III domain; TK, tyrosine kinase catalytic domain. (b and c) Summary of sequencing results from animals injected with four different sgRNAs in combination with vasa-Cas9 plasmid. There were n = 3 sequencing libraries per sgRNA. The data are presented as the means ± SEM, $^*P < 0.05$ (Student's *t*-test). (b) Quantification libraries as a percentage of aligned reads containing an indel (insertion or deletion) at the target sequence and (c) percentage of reads that cause frameshift mutations. (d) Representative sequencing results of CRISPR/Cas9-generated deletion mutations in the *Nl*InR1 locus using three sgRNAs separately from different individual mutants. Deletions are shown as dashes, insertions and PAM are labeled in green and blue, respectively. (For interpretation of the references to colour in this figure legend, the reader is referred to the Web version of this article.)

plasmid.

The sgRNA transcription is typically driven by the RNA polymerase III-dependent U6 promoters *in vivo*. The U6 promoter is commonly used to transcribe a variety of small RNAs with precisely defined 5′ and 3′ ends, which are suitable for sgRNAs with a ubiquitous and high-level expression (Mali et al., 2013). Although U6 promoters have been isolated in many organisms, no equivalent promoter had been described previously in BPH. We identified U6 snRNA genes in the BPH and cloned three putative upstream and downstream regulatory sequences of the U6 genes, finally generating three versions of plasmids for expression of sgRNA, named U6a, U6b, and U6c (Fig. 1b). The U6 promoter prefers guanine as the transcription initiation site for optimal transcription and can thus be used to target the sequence in the form of 5′G-N19-NGG-3' (Jinek et al., 2013). Subsequent studies showed that extra nucleotides mismatched at the 5′ end of the sgRNA can be tolerated. Thus, with our sgRNA expression plasmids, the constraint on the selection of target sequences in the genome can be circumvented by appending a G before the target sequence that conforms to 5′G-N20-NGG-3'.

We first assessed the expression of the vasa-Cas9 and U6 plasmids by separate transfection of High Five cells (Invitrogen, Carlsbad, CA, USA). The cells were harvested 48–72 h post-transfection. The expression of Cas9 protein was detected by Western blotting analysis (Supplementary Fig. S4b). U6 plasmid expressions were confirmed by qRT-PCR with specific primer pairs for a heterologous sequence in our entry vector. As expected, our vector setting displayed high expression in High Five cells (Supplementary Fig. S4c), meanwhile different U6 plasmids differ in their transcriptional activity, with U6a and U6b exhibiting higher activity than U6c.

3.2. Evaluating optimal injection sources for CRISPR/Cas9 mutagenesis in *Nl*InR1 locus

We tested the activity of driven of the U6a and U6b plasmids at an endogenous locus in the BPH genome. These two plasmids were constructed to separately target the coding sequence of the *Nl*InR1 gene at two targets (T1, T2) (Fig. 2a). A single U6 plasmid and the vasa-Cas9 plasmid were coinjected into BPH embryos. G_0 animals were reared from hatching to the adult stage. We performed deep sequencing of indexed PCR amplicons surrounding Cas9 target regions from pools of G_0 adults to accurately determine the mutation rates after they were outcrossed with WT BPH. Following sequencing, we found that the U6a-T2 plasmid gave a maximum mutation rate of 11.2%, while U6b-T2 yielded a maximum mutation rate of 7.2%. The mutagenesis rate of T1 was lower than that of T2 in tested injections, but the U6a-T1 plasmid still yielded higher targeting efficiencies than U6b-T1 (Fig. 2b and c). Thus, we stress the necessity of designing and testing effective mutations of multiple sgRNAs at an early stage before large-scale knockout studies. To examine whether these mutations could also be stably transmitted through the germline, we amplified the targeted region derived from outcrossed G_0 offspring for deep sequencing. Strikingly, the overall heritable mutation rates revealed that U6a was approximately twice as effective as the U6b plasmid in both T1 and T2 (Table 1). Collectively, our results demonstrate that U6a and U6b promoters differ substantially in targeting efficiencies in both somatic cells and the germline, with the BPH U6a promoter having the strongest activity in mediating efficient gene targeting. Thus, we used the U6a plasmid in all subsequent constructs.

We next sought to identify Cas9/sgRNA combinations to determine an optimal injection mix for germline transmission of mutations in *Nl*InR1. We performed similar experiments targeting either T1 or T2 of the *Nl*InR1 locus with Cas9/sgRNA ribonucleoprotein (RNP) complex and found that nearly 99% of the G_0 embryos failed to hatch. We found a much higher survival rate (up to 10.5%) of G_0 embryos after injection of either sgRNA plasmid. Cas9 RNP treatment resulted in substantial lethality, with only 38% overall of hatched embryos progressing to adulthood. As a comparison, the survival rate was approximately twice as high as that of Cas9 RNP in vasa-Cas9- and U6 plasmid-treated

Table 1
Somatic and germline mutation rates using different CRISPR/Cas9 constructs on *Nl*InR1 locus.

Injection sources	Embryos, n	Hatched eggs	Survival, %	Adult	Fertile	Germ-line mutants, n, %[a]
vasa-Cas9, U6a-T1	410	35	8.5	30	25	5, 20.0
vasa-Cas9, U6b-T1	390	41	10.5	38	33	3, 9.1
Cas9 Protein, sgRNA-T1	584	6	1.0	2	2	2, 100
vasa-Cas9, U6a-T2	492	29	5.9	19	14	5, 35.7
vasa-Cas9, U6b-T2	475	32	6.7	22	18	3, 16.7
Cas9 Protein, sgRNA-T2	524	7	1.3	3	2	1, 50.0

[a] The germline mutants were calculated as the proportion of fertile G_0 BPH that gave rise to mutant progeny.

embryos. However, Cas9 RNP-induced germline mutation rates were significantly higher than those of vasa-Cas9 at two distinct target sites among surviving G_0 adults. Of 2 G_0 fertile survivors at T1, 2 inherited the mutation allele. The mutation allele was found in 1 out of 2 fertile survivors at T2 (Table 1). PCR amplification of the target region from surviving G_0 animals revealed detectable rates of insertions or deletions surrounding the Cas9 cut site (Fig. 2d). These results suggest that vasa-Cas9 allows efficient germline transmission of mutations and improved survival rate to adulthood compared with Cas9 protein. Taken together, our results show that the combination of vasa-Cas9 and U6a plasmid appears to provide an optimal Cas9 and sgRNA source for genome editing of BPH genes that are essential for viability.

3.3. Loss of function in NlInR1 induces pleiotropic phenotypes

We found that the *Nl*InR1 gene is essential in the soma for the development of BPH to adult stages. Homozygous genotypes for mutant *Nl*InR1 are embryonic lethal, but the heterozygous *Nl*InR1$^{E6b/+}$ (mutations at T2 target) resulted in viable, smaller adults with a marked delay in development. In the G_1 generation, *Nl*InR1$^{E6b/+}$ mutants eclose 4–6 days after their WT siblings (Fig. 3a). We performed a detailed developmental study to reveal which stage of development is delayed in the *Nl*InR1$^{E6b/+}$ mutants. The mutants exhibit significantly prolonged fourth and fifth instars relative to WT nymphs (Fig. 3b). This finding implies that development during particular phases is highly sensitive to decreased *Nl*InR1 activity. The average body weight is reduced to 89% in female mutants and 86% in male mutants compared with 1-day-old WT adults (Fig. 3c, Fig. 4a–d). Although body length and pronotum width were reduced in 1-day-old male/female adults, the body proportion of mutants were similar to those of WT. Interestingly, we found that the adult wing size was obviously smaller than that of WT short-winged adults, reducing the average wing size to 63% and 61% in females and males, respectively (Fig. 3d and 4e, f). Under outcrossing conditions (G_1 mutant progeny were crossed with WT animals), the fecundity of *Nl*InR1$^{E6b/+}$ females was reduced severely to 48% of that of WT (Fig. 3e). Meanwhile, a significant decrease in fecundity was already observed in young 5-day-old mutant females (Fig. 3e), we speculated that low expression of *Nl*InR1 compromises fecundity and at least some form of developmental defect is caused in germline cells. The overall hatching rates were greater than 92% in WT at 26 °C, whereas *Nl*InR1$^{E6b/+}$ exhibited a hatching rate of 61% (Fig. 3e). We investigated whether *Nl*InR1 abundance contributes to lifespan in BPH. We found that mutants with only one functional *Nl*InR1 allele significantly outlived the WT controls. In females, the maximum lifespan of the *Nl*InR1$^{E6b/+}$ mutants was 36% longer than that of WT females (Fig. 3f), whereas males of *Nl*InR1$^{E6b/+}$ were 33% more long-lived than the WT controls (Fig. 3g).

InR is highly pleiotropic in many organisms; therefore, we characterized multiple independently generated lines of *Nl*InR1 mutants using three sgRNAs (T1, T2, and T3) that target two distinct domains of the *Nl*InR1 gene to investigate its loss-of-function phenotype (Fig. 2a). We observed similar results in three independent *Nl*InR1 knockout lines at each target site, which were found to have frameshift mutations in the coding sequence of *Nl*InR1 and to be viable and fertile when heterozygous with decreased adult body weight and wing size in both males and females (Fig. 2d, Table S2). All three mutant lines are recessive lethal, suggesting that the heterologous *Nl*InR1 multimers are at least partially functional. These three *Nl*InR1$^{-/+}$ mutant lines transmitted the mutant allele in accordance with Mendelian inheritance (47%, n = 685). Surprisingly, all *Nl*InR1$^{E4/+}$ mutants show severe malformation of the adult forewings, leaving the wing vein and bristles apparently lost (Fig. 4g and h). The average wing size of heterozygous *Nl*InR1$^{E4/+}$ (mutation at the T3 target) was severely reduced to 39% in females and only 30% in males compared to WT, but the average male/female body weight reduction was similar to those of *Nl*InR1E$^{6b/+}$ mutants (Fig. 4i). Our T1 and T2 targets were located in the furin-like cysteine-rich (Fu) domain, which involves receptor aggregation, whereas the T3 target was within the leucine-rich repeat (receptor L) domain that functions in ligand-binding (Fig. 2a). Measurement of *Nl*InR1 autophosphorylation revealed that all of three *Nl*InR1$^{-/+}$ mutant lines confer reduced autophosphorylation activity. The autophosphorylation activity of *Nl*InR1$^{E6b/+}$ and *Nl*InR1$^{E6a/+}$ mutants (mutations at T1 target) was reduced to 53% and 55% of that of the WT, respectively. However, only to 40% in *Nl*InR1$^{E4/+}$ mutants, implying that *Nl*InR1 activity is strongly inhibited with the low ligand-binding activity (Fig. 5a). Taken together, these results indicated that a general decrease in *Nl*InR1 levels can affect growth and development, lifespan, and reproduction in BPH.

3.4. A reduction of insulin signaling in NlInR1 mutants

We investigated the factors underlying BPH heterozygosity for a mutation that may exhibit a detectable decrease in either mRNA expression or the amount and function of *Nl*InR1 protein. We analyzed the expression pattern of insulin signaling in 1-day-old *Nl*InR1$^{E6b/+}$ females. As expected, qRT-PCR analyses revealed that the relative expression level of *Nl*InR1 was highly reduced (29% of the WT), but that *Nl*InR2 transcripts were not significantly changed compared to the WT controls (Fig. 6a). We then investigated how the reduced *Nl*InR1 levels affected downstream intracellular signalling. The relative expression of *Nl*Chico, a major substrate of *Nl*InR1, was reduced to 54%. In *D. melanogaster,* phosphatidylinositol 3 kinase (PI3K) binds Chico to recruit phosphoinositide-dependent protein kinase (PDK1) and Akt to the membrane to phosphorylate phosphatidylinositol-4,5-bisphosphate (PIP 2) to phosphatidylinositol 3,4,5-trisphosphate (PIP 3), leading to the phosphorylation and activation of Akt by PDK1 (Oldham and Hafen, 2003). Activated Akt regulates multiple cellular processes via several related effectors, which mainly include glycogen synthase kinase 3 (GSK3), transcriptional factor forkhead box class O (FOXO), target of rapamycin (TOR) and p70 ribosomal S6 kinase (S6K). Notably, in *Nl*InR1$^{E6b/+}$ mutants, *Nl*PI3K expression was reduced to 40% of the WT, the expression levels of *Nl*PDK1 and *Nl*Akt were decreased to 42% and 55%, respectively (Fig. 6b). Moreover, the expression levels of *Nl*FOXO exhibited a decrease to approximately 39% of control levels and two of the key FOXO targets, *Nl*4EBP and *Nl*Bmm, were significantly reduced to 48% and 45%, respectively, compared to WT (Fig. 6c). *Nl*TOR and *Nl*S6K also exhibited a severe decrease to approximately 45% and 41% of WT in the mutants, respectively (Fig. 6d).

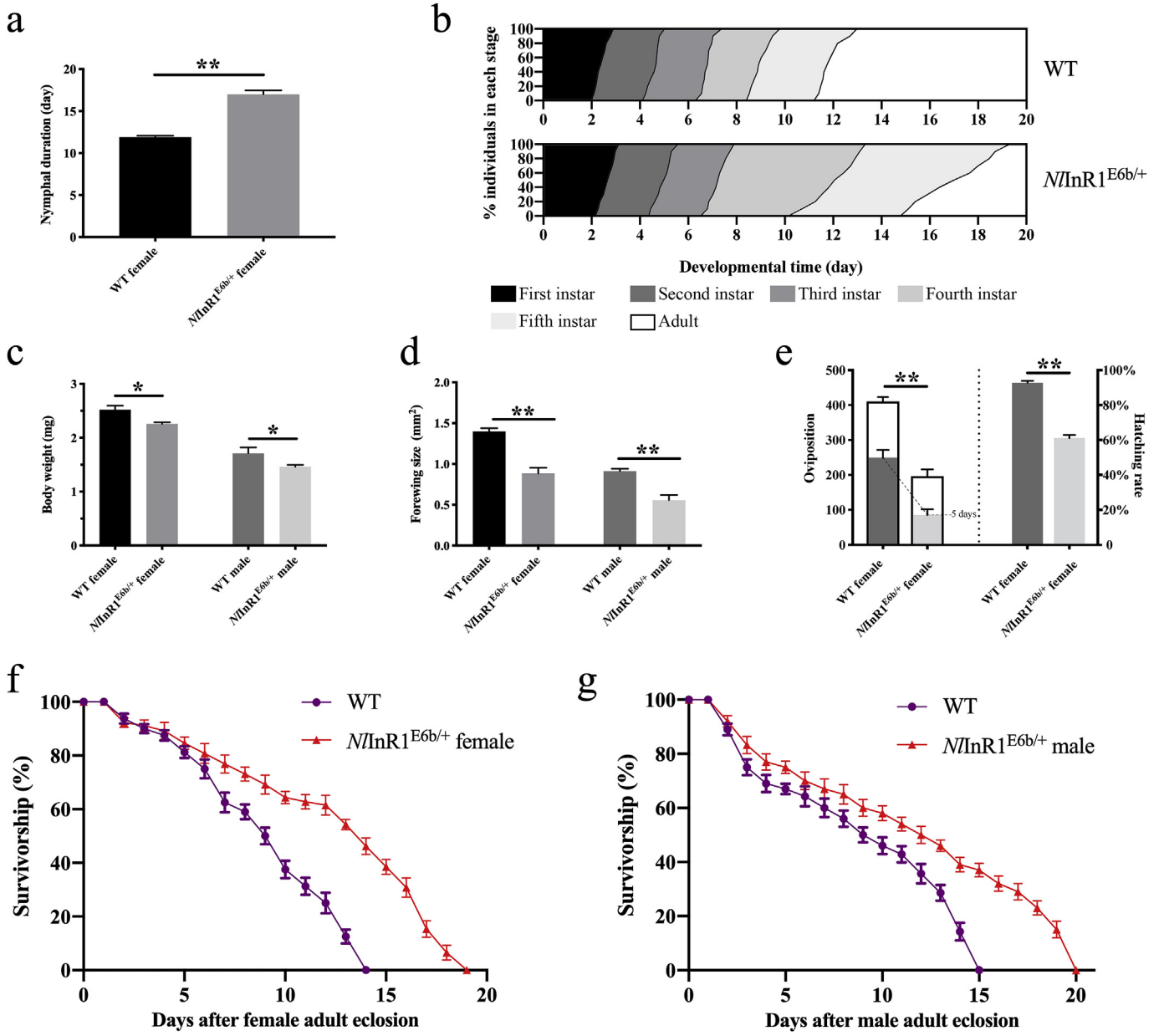

Fig. 3. *Nl*InR1 regulates growth and lifespan. (a) *Nl*InR1 mutants exhibit prolonged nymphal development. (b) Developmental delay in *Nl*InR1 mutants occur primarily through elongation of the fourth- and fifth-instar nymph stage. The curve among different developmental stages indicates the molting ratio. (c) *Nl*InR1 mutant adults show reduced body weight compared to both male and female controls. (d) The forewing size of *Nl*InR1 mutant BPHs was reduced compared to that of the controls. (e) Average fecundity and hatching rate of WT and *Nl*InR1 mutant females. (f and g) Survivorship of *Nl*InR1 mutants was increased relative to that of the WT among females (f) and males (g) (log-rank test, $P < 0.01$). (a, c-g) Data are presented as the mean ± SEM. $^{*}P < 0.05$, $^{**}P < 0.01$ (Student's *t*-test).

We next performed immunoblot analysis from 1-day-old females to compare the abundance of IIS signaling in *Nl*InR1$^{E6b/+}$ mutants to that in the WT. The mutants showed a 40% decrease in the abundance of *Nl*Akt compared to that in WT, suggesting a defective kinase function in the *Nl*InR1$^{E6b/+}$ mutants (Fig. 5b). Western analysis also showed a similar reduction level in *Nl*InR1-induced phosphorylation of *Nl*Akt in mutants, to 58% of that in WT (Fig. 5b). Consistently, *Nl*InR1-stimulated phosphorylation of two important pathways activated by the *Nl*Akt signaling cascade, *Nl*FOXO and *Nl*S6K, was reduced to 60% and 42% in mutants, respectively, indicating that it is sufficiently sensitive to detect a loss-of-function mutation in heterozygous mutants of the *Nl*InR1 locus (Fig. 5c and d). The expression levels and abundance of these genes among males with the *Nl*InR1$^{E6b/+}$ genotype follow the pattern observed for females (data not shown). Thus, the deficiency in growth and the loss of IIS activity strongly supporting the CRISPR/Cas9 loss-of-function phenotype for *Nl*InR1. Together, these results suggested that *Nl*InR1 haploinsufficiency downregulates the IIS pathway.

3.5. Global expression profiling of adult female in NlInR1 mutants

To comprehensively investigate the impact of IIS suppression by *Nl*InR1 mutation, we used RNA-Seq to compare transcript abundance in WT (short-winged morphs) and *Nl*InR1$^{E6b/+}$ mutants. We sampled female adult BPHs (0–12 h after eclosion) of both WT and strong knockout phenotypes. Before expression profiling analysis, we first measured the expression level of *Nl*InR1 in mutants and only used samples with the lowest *Nl*InR1 transcripts for further sequencing. The pairwise correlations of the RNA-Seq datasets between the replicates from two groups were high ($r > 0.96$) (Fig. 7a). In *Nl*InR1 mutants, of 12,981 expressed genes, 1857 (14.3% of all expressed genes)

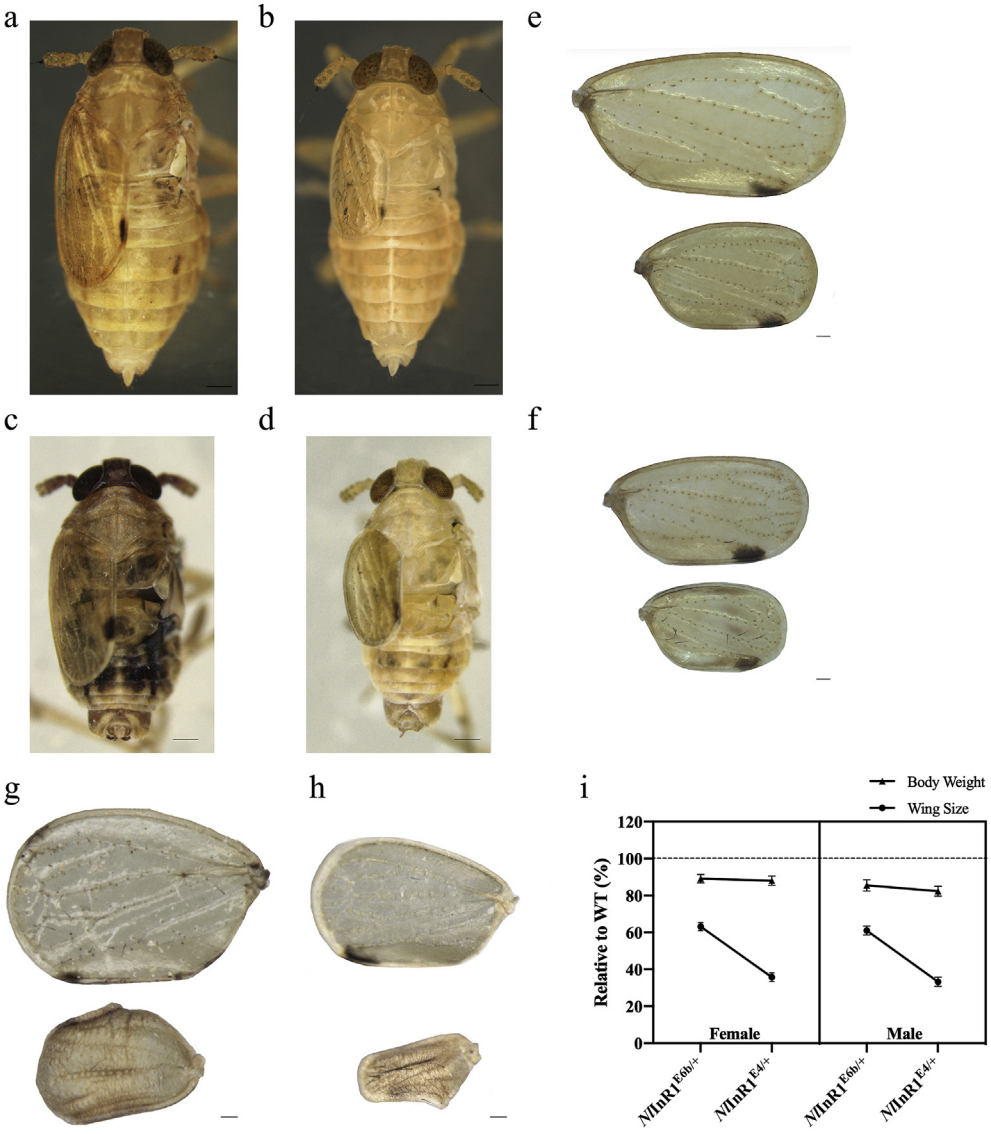

Fig. 4. *Nl*InR1 mutant BPHs show a reduced body size and forewing size. (a) WT female adult. (b) *Nl*InR1$^{E6b/+}$ female adult. (c) WT male adult. (d) *Nl*InR1$^{E6b/+}$ male adult. (e) *Nl*InR1$^{E6b/+}$ mutant displays smaller forewing size than WT control. top: WT female adult, bottom: *Nl*InR1$^{E6b/+}$ female adult. (f) Comparison of forewing between WT control and mutant male. top: WT male adult, bottom: *Nl*InR1$^{E6b/+}$ male adult. (g) Forewing of WT (top) and *Nl*InR1$^{E4/+}$ mutant female. (h) Forewing of WT (top) and *Nl*InR1$^{E4/+}$ mutant male. (i) Relative reduction of forewing size and body weight of mutants compare to WT. a-d, scale bars indicate 100 μm; e-h, scale bars indicate 200 μm.

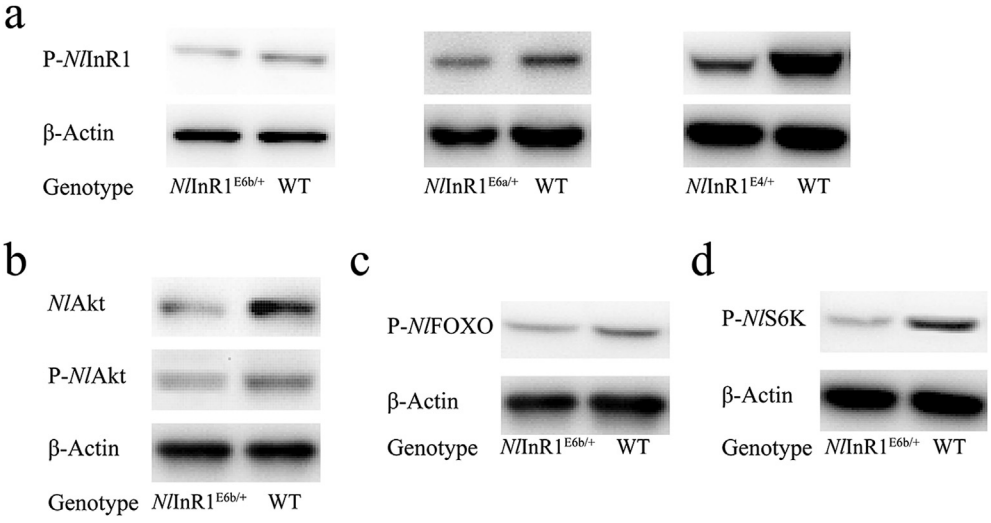

Fig. 5. Lack of *Nl*InR1 expression in mutants reduces activation of major intracellular signaling pathways by Western blotting analysis. (a) Phosphorylation of *Nl*InR1 was reduced in three *Nl*InR1 mutant lines. (b) The expression levels of phospho-*Nl*Akt (P-*Nl*Akt) and *Nl*Akt were reduced in *Nl*InR1 mutants. (c and d) *Nl*InR1-induced activation of *Nl*FOXO and *Nl*S6K was also reduced in *Nl*InR1 mutants. Each experiment was performed in triplicate, and band intensities were quantified from 3 biological replications.

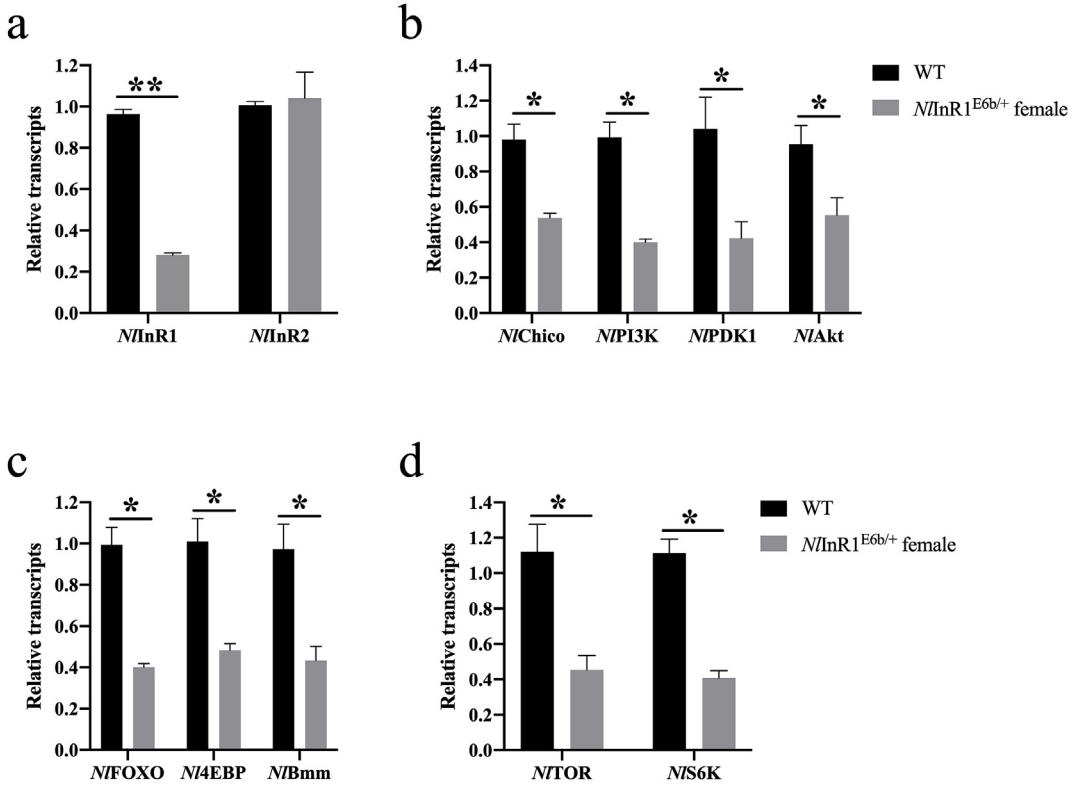

Fig. 6. A reduction of insulin signaling in *Nl*InR1 mutants. (a–d) *Nl*InR1, *Nl*InR2, *Nl*Chico, *Nl*PI3K, *Nl*PDK1, *Nl*Akt, *Nl*FOXO, *Nl*4EBP, *Nl*Bmm, *Nl*mTOR and *Nl*S6K expression levels were analyzed by qRT-PCR in 1-day-old females. Data represent three biological replicates with three technical replicates, and each replication contains 5 females. The data are shown as the mean ± SEM. $^{*}P < 0.05$, $^{**}P < 0.01$ (Student's *t*-test).

differentially expressed genes (DEGs) (|log2 (fold change)| > 1.4, *P*-value < 0.05) were identified, 606 (4.7%) unigenes were upregulated and 1251 (9.6%) were downregulated compared to WT BPHs (Fig. 7b, Table S3). Thus, a large proportion of measured genes exhibited significantly changed expression in our comparison, indicating that partial loss of *Nl*InR1 represented drastic changes for BPH and that *Nl*InR1-regulated signaling was potentially involved in a large gene network. Ten randomly selected DEGs were further analyzed by qRT-PCR to validate the reliability of RNA-Seq results, demonstrating a high correlation between the qRT-PCR results and the RNA-Seq analysis (Supplementary Fig. S6). According to the Gene Ontology (GO) enrichment analysis, we noted that a larger proportion of downregulated genes were significantly enriched in a diverse array of GO terms, such as mitotic chromosome condensation, septate junction, transporter activity, calcium ion binding and fatty acid biosynthetic process (Fig. 7c, adjusted *P*-value < 0.05, Table S4). By contrast, upregulated genes were not preferentially enriched in any particular GO category. We also examined the pathways affected by the DEGs by annotating to the Kyoto Encyclopedia of Genes and Genomes (KEGG) database, which showed that the majority of enriched KEGG pathways included functions related to lipid and carbohydrate metabolism and amino acid and nucleotide biosynthesis (Fig. 7d, Table S5), reflecting the important role of *Nl*InR1 in cell development homeostasis. The affected pathways also included those related to insulin resistance, phototransduction, the Wnt signaling pathway, the phosphatidylinositol signaling system and endocytosis. These results revealed that *Nl*InR1 has pleiotropic functions in BPH, showing evidence that the suppressed IIS affects both metabolism and growth.

4. Discussion

Given the explosive pace of research employing the CRISPR/Cas9 system, it has been widely used for genomic engineering in a large variety of organisms and this breakthrough technology provides a highly effective and robust tool compared to ZFN- and TALEN-mediated mutagenesis. Although a proof-of-principle study has demonstrated CRISPR/Cas9-mediated mutagenesis in BPH (Xue et al., 2018), a systematic assessment of different CRISPR/Cas9 combinations has not been described. Previous studies have found that Cas9 RNP can induce mutations with higher frequencies than other delivery methods (Gaj et al., 2017; Kim et al., 2014; Zuris et al., 2015). In the current study, we verified that compared to Cas9 RNP, Cas9 and sgRNA expressed from plasmids promote high heritable loss-of-function efficiency and ideal survival rate in G_0 animals for the *Nl*InR1 gene in BPH. The advantage of the approach that we describe herein is the low somatic mutations by introducing vasa-Cas9. No visible phenotypes were observed in our G_0-injected BPH, most likely because Cas9 expression was germline restricted by the *Nl*vasa promoter rather than the substantial activity in both somatic and germline cells observed with the Cas9 protein. Thus, we deduce that a relatively low level of somatic mutation events in somatic tissues can circumvent the potentially deleterious effects when the target gene is related to cell viability or growth. Specifically, we characterized three U6 promoters for the first time in BPH. *In vivo* experiments using deep sequencing revealed that, of the U6a and U6b promoters, the U6a promoter leads to the strongest sgRNA activity and germline transmission rates. This observation suggests that our optimized system using vasa-Cas9 in combination with U6a-sgRNA plasmid can be used to transmit mutations through the germline with remarkably high efficiency and lends support for further loss-of-function studies in essential genes in BPH. It has been reported that the transgenic CRISPR/Cas9 system in which Cas9 and sgRNA integrated into the genome of *Drosophila* had up to a 100% transmission rate of the target gene (Kondo and Ueda, 2013; Port et al., 2014). However, the rate of transgene inheritance using microinjection-based CRISPR/Cas9 components by plasmid in our study was less than 50% (Table 1). We suggest that our plasmids are suitable for the construction of fully

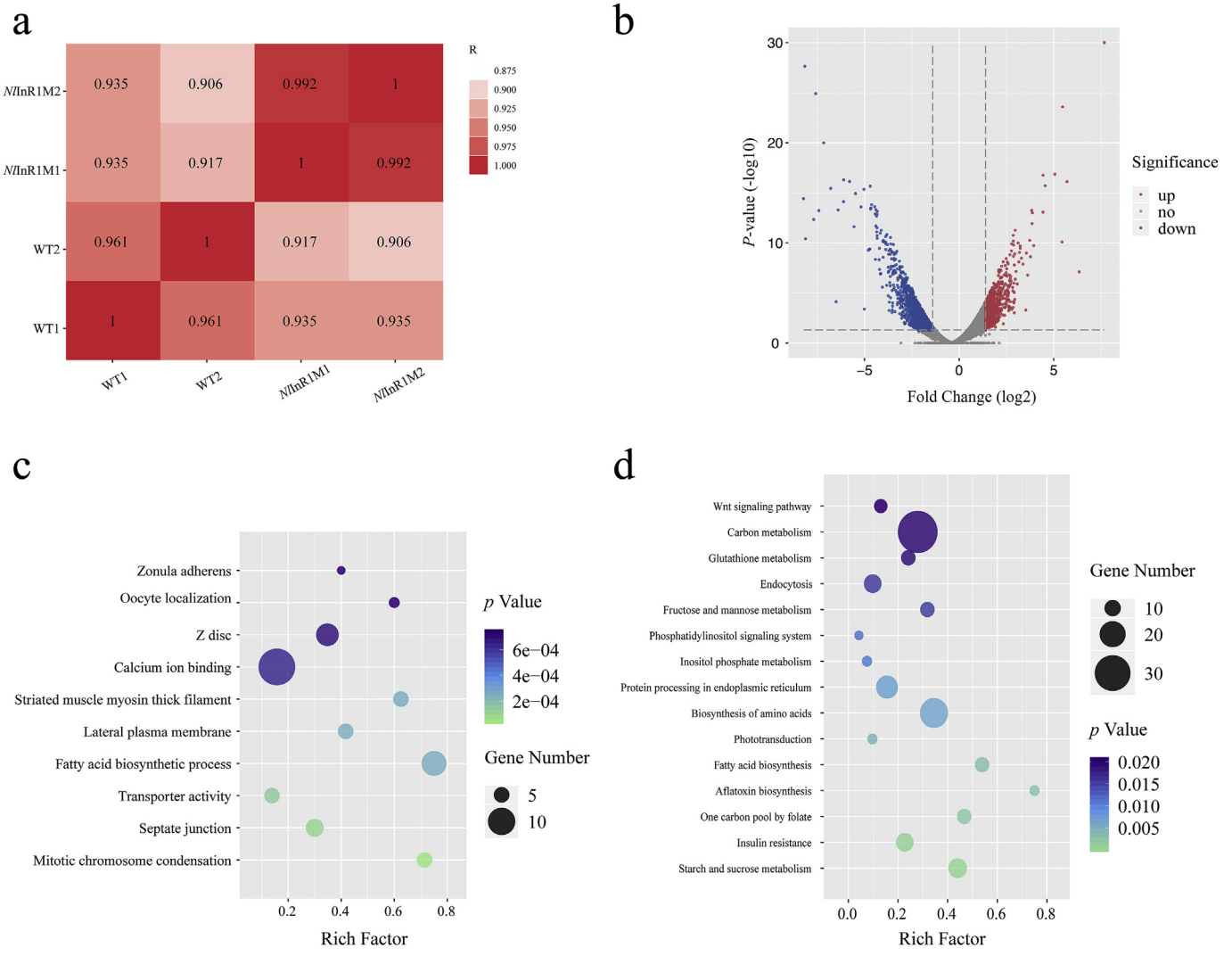

Fig. 7. RNA-Seq analysis reveals transcriptomic profiles in *Nl*InR1 mutants compared to WT. (a) The correlation heatmap between samples. The correlation was calculated according to the Pearson correlation coefficient. WT: wild type; *Nl*InR1M: *Nl*InR1 mutant. (b) Volcano plots of individual gene expression levels between *Nl*InR1 mutants and WT controls. Differentially expressed genes (DEGs) (|log2 (fold change)| $>$ 1.4, $P < 0.05$) are in red (upregulated) and blue (downregulated), dashed lines indicate the threshold value. (c) The top 10 significantly enriched categories of GO enrichment analysis of DEGs. (d) The top 15 enriched KEGG pathways by annotating to the KEGG database of DEGs. (For interpretation of the references to colour in this figure legend, the reader is referred to the Web version of this article.)

transgenic CRISPR/Cas9 lines for further study to achieve highly specific and consistent genome modifications. Importantly, a transgenic line expressing Cas9 in the germline (vasa-Cas9) only needs to be injected with our easy-to-make sgRNA-expression plasmids into the embryos. This one-step approach, which can achieve simultaneous multiplex gene knockout by injecting multiple sgRNAs, will facilitate the production of diverse mutant lines and be beneficial for the analysis of gene networks in this nonmodel organism. Furthermore, CRISPR/Cas9-based studies will be particularly powerful if mutagenesis can be restricted at the temporal and spatial levels. We have taken a step in this direction, further study can combine our expression cassette with the Gal4/UAS system to target within a defined group of cells.

Our optimized Cas9/sgRNA system will facilitate homologous recombination (HR)-mediated knock-in to expand the applications using an extra donor DNA as previously described (Kistler et al., 2015). For example, a fluorescent marker gene can be introduced when transgenic progenies are not easily identifiable, site-directed mutagenesis can be employed to alter activity-critical residues in proteins, an ectopic tag can be introduced in endogenous loci to detect gene expression patterns. The vasa-Cas9 and U6-sgRNA developed in this study may also bring us one step closer to the construction of an effective CRISPR/Cas9-based gene drive system (Gantz et al., 2015; Hammond et al., 2016). Gene drive systems are attracting increasing interest as alternative improvements to traditional nonselective methods for insect pest management. CRISPR/Cas9-mediated gene drive for pest control may be more advanced than any other proposed genetic control method, with high species specificity and cost-effectiveness. To date, most Cas9 cassettes of the CRISPR/Cas9-mediated gene drive systems are expressed under the vasa promoter originally developed from *D. melanogaster* (Gantz and Bier, 2015), which is active in both male and female germline (Van Doren et al., 1998). However, vasa also functions outside of the germlines, these somatic functions could lead to a high frequency of non-homologous end-joining (NHEJ) and drive-resistant loci following double strand break (DSB) (Bourgeois et al., 2016). Notwithstanding, it remains to be determined whether our vectors will be effective in a gene drive system in BPH. It would be straightforward to develop a transgenic vasa-Cas9 line crossed with a split sgRNA drive transgenic line and measure the rates of inheritance following the stringent confinement strategies for safe gene drive (Akbari et al., 2015).

The *Nl*InR1 is homologous to the mammalian IR/IGFR and has a similar structure to that of its mammalian counterpart. Complete loss of *Nl*InR1 function resulted in embryonic lethality, while partial loss of *Nl*InR1 function dramatically affected development, wing growth, body size and lifespan (Figs. 3 and 4). These growth effects are comparable to the absence of components of the IIS such as InR, Chico, Dp110, Akt, Rheb and PI3K in *Drosophila* (Murillo-Maldonado et al., 2011). Moreover, our findings are consistent with the IGF1, IR/IGF-1R and IRS1 knockout mutants in higher animals, indicating that the branch points of IIS have been functionally conserved during evolution. Numerous observations underscore the importance of the InR/PI3K/Akt pathway in controlling the size and growth of tissues (Hietakangas and Cohen, 2009). Akt has been demonstrated to be a major mediator of the InR/PI3K/Akt-mediated growth regulation that affects cellular growth and body size (Brazil and Hemmings, 2001; Umemiya-Shirafuji et al., 2012). Analysis of our *Nl*InR1 mutations has shown that partial loss-of-function of *Nl*InR1 reduces activation of major intracellular signaling pathways (Figs. 5 and 6), indicating that severely suppressed InR/PI3K/Akt signaling pathway causes defective growth of BPH. We noted that a large proportion of genes in the IIS pathway were significantly downregulated at the mRNA and protein levels. A similar result was reported in mice, lack of IGF-1R displays suppressed activity of IIS in cultured mouse embryonic fibroblasts (Holzenberger et al., 2003). These results demonstrated that IIS conservation occurs at the physiological level. Interestingly, in our study, the mutant phenotype was much more severe than observed with previously reported RNAi treatment of *Nl*InR1 (Xu et al., 2015). For example, the wing size in the heterozygous mutant was significantly reduced by approximately 40%–60% depending on the target site, but the rate was 10% in RNAi experiments. Importantly, the 40% reduction resembled the silencing effect of the ds*Nl*Akt phenotype, suggesting that InR/PI3K/Akt signaling activity plays a key role in the regulation of wing size, temporary suppression of *Nl*InR1 by RNAi only led to incomplete downregulation of the inducible insulin/Akt signaling pathway. Moreover, the lower expression of *Nl*Akt (60% of WT) and abundance of phosphorylated *Nl*Akt (p-*Nl*Akt; 58% of the WT) in *Nl*InR1 mutants suggested that the effect of Akt is important in the transmission of the insulin signal. The gene expression in our study was determined in the whole adult BPH bodies, we believe that there must have compensatory mechanisms in these signaling molecules, which may be involved in some tissues or cells. Tissue-specific versus generalized gene targeting of the signaling molecules should be focused in further study. As is the case for target gene knockouts by CRISPR/Cas9, our results show that the RNAi effect is moderate or temporary. Thus, some RNAi phenotypes in BPH may be incompletely penetrant or missed altogether because of a partial reduction of the corresponding transcript expression level of the target gene. The *Nl*InR1 knockout by our optimized CRISPR/Cas9 system provides a more comprehensive tool for functional and phenotypic analysis. Moreover, our findings uncover a complex mechanism of *Nl*InR1 regulation in body and wing size, suggesting that the severity of the mutant phenotype is variant when targeting different exons or domains. And the difference in wing size between *Nl*InR1$^{E4/+}$ and *Nl*InR1$^{E6b/+}$ mutants strongly suggested that such size is dose-dependent, reflecting tissue-specific plasticity in gene regulation. To our knowledge, this is the first report of such differences in BPH.

IIS is initiated by InR, leading to the eventual activation of downstream components, including PI3K, Akt, and FOXO. Akt can induce various downstream components, one of which is the transcription factor FOXO that is directly inactivated by Akt (Puig and Tjian, 2005). FOXO is an important homeostatic mechanism of the IIS cascade. In *C. elegans*, dampening the DAF-2 insulin receptor-like signaling pathway results in increased longevity, in part through the nonautonomous FOXO worm orthologue DAF-16 (Kenyon et al., 1993). For *Drosophila*, deficiency in the IIS can extend lifespan, which is dependent on FOXO, whereas reduced reproduction and body size and delayed development are not (Slack et al., 2011). Interestingly, a remarkably similar phenotype is observed in mammalian aging that effects the insulin receptor (Brüning et al., 2000). The TOR signaling pathway is also an important regulatory target of IIS. The IIS and TOR signaling pathways interact with each other, forming a complex network that has been associated with longevity and aging (Kenyon, 2010). Mutations that reduce the activity of TOR can also extend lifespan in yeast, worms, flies and mice (Fabrizio et al., 2001; Hansen et al., 2007; Kapahi et al., 2004; Selman et al., 2008), suggesting that TOR signaling is a most evolutionarily conserved lifespan-extending pathway. In *Drosophila*, dominant-negative forms of TOR or S6K result in extended lifespan and anti-aging effects, which rely on both upregulated autophagy and downregulated S6K (Bjedov et al., 2010). In addition, TOR can negatively regulate IIS through S6K and its activity is required to activate Akt (Radimerski et al., 2002). It will be interesting to explore the role of the IIS/TOR network in regulating the development and longevity of BPH. We found that phosphorylation of two important pathways activated by the *Nl*Akt signaling cascade, *Nl*FOXO and *Nl*S6K, was reduced in *Nl*InR1 mutants (Fig. 5). These observations indicate that suppressed IIS inhibits the activity of the TOR target S6K and that reduced IIS/TOR activity was caused by a reduction in *Nl*InR1 signaling probably in a *Nl*Akt-independent fashion. The concordance of phenotypes of increased lifespan in *Nl*InR1 mutants suggests that *Nl*FOXO and *Nl*S6K may be central to a common mechanism among animals for the regulation of longevity. Our *Nl*InR1 mutant lines provide a valuable tool for future research of the lifespan regulatory mechanisms. However, since there is considerable crosstalk between the IIS and TOR signaling pathways, it will now be important to investigate how lifespan regulation is achieved through IIS in BPH. One clue comes from studies indicating that InR can affect specific neurosecretory tissue for the secretion of juvenile hormone (JH) (Liu et al., 2016; Tatar et al., 2001), in which the neuroendocrine regulation of metabolism by IIS may be focused.

InR signaling plays a key role in physiology and has been widely studied in multiple species, but the genome-wide transcriptional response to mutations in *Nl*InR1 signaling pathway in BPH remains poorly understood. Here, we carried out an RNA-Seq analysis of female adult (0–12 h after eclosion) from both *Nl*InR1 mutants and WT BPHs. Specifically, we found *Nl*InR1 association with pleiotropic networks that modulate gene expression since the DEGs are highly enriched for functions important for growth and development, metabolism, biosynthesis, nervous system function and cell fate (Fig. 7). Our data suggest that these effects have considerable relevance in insulin-related phenotypes. Moreover, the reduced phototransduction pathway revealed that neuronal communication is compromised in *Nl*InR1 mutants, which is usually caused by reduced neurotransmitter release. We found the inositol 1,4,5-trisphosphate receptor (itpr) involvement in this process was significantly differentially expressed between mutants and WT. Itpr is required for flight and associated neuronal rhythmicity through modulating serotonin and/or dopamine release (Banerjee et al., 2004; Vermassen et al., 2004). This finding may help us uncover an upstream regulator of *Nl*InR1 in further studies. Finally, our data suggest that *Nl*InR1 may be central in the neuroendocrine regulation of metabolism and biosynthesis and that mutation has associated consequences upon growth and aging. Environmentally triggered phenotypic plasticity of BPHs is likely guided by neural circuits at a cellular level. DEGs in our study may provide a rich source involved in sensing environmental information to physiological processes, further studies are needed to verify whether these links are correlative or causative.

Acknowledgements

This work was supported by the National Natural Science Foundation of China (31730073).

Appendix A. Supplementary data

Supplementary data to this article can be found online at https://doi.org/10.1016/j.ibmb.2019.103246.

References

Akbari, O.S., Bellen, H.J., Bier, E., Bullock, S.L., Burt, A., Church, G.M., Cook, K.R., Duchek, P., Edwards, O.R., Esvelt, K.M.J.S., 2015. Safeguarding gene drive experiments in the laboratory. Science 349, 927–929.

Banerjee, S., Lee, J., Venkatesh, K., Wu, C.-F., Hasan, G., 2004. Loss of flight and associated neuronal rhythmicity in inositol 1, 4, 5-trisphosphate receptor mutants of *Drosophila*. J. Neurosci. 24, 7869–7878.

Belfiore, A., Frasca, F., Pandini, G., Sciacca, L., Vigneri, R., 2009. Insulin receptor isoforms and insulin receptor/insulin-like growth factor receptor hybrids in physiology and disease. Endocr. Rev. 30, 586–623.

Bjedov, I., Toivonen, J.M., Kerr, F., Slack, C., Jacobson, J., Foley, A., Partridge, L., 2010. Mechanisms of life span extension by rapamycin in the fruit fly *Drosophila melanogaster*. Cell Metabol. 11, 35–46.

Bourgeois, C.F., Mortreux, F., Auboeuf, D., 2016. The multiple functions of RNA helicases as drivers and regulators of gene expression. Nat. Rev. Mol. Cell Biol. 17, 426–438.

Brazil, D.P., Hemmings, B.A., 2001. Ten years of protein kinase B signalling: a hard Akt to follow. Trends Biochem. Sci. 26, 657–664.

Brogiolo, W., Stocker, H., Ikeya, T., Rintelen, F., Fernandez, R., Hafen, E., 2001. An evolutionarily conserved function of the *Drosophila* insulin receptor and insulin-like peptides in growth control. Curr. Biol. 11, 213–221.

Brüning, J.C., Gautam, D., Burks, D.J., Gillette, J., Schubert, M., Orban, P.C., Klein, R., Krone, W., Müller-Wieland, D., Kahn, C.R., 2000. Role of brain insulin receptor in control of body weight and reproduction. Science 289, 2122–2125.

Fabrizio, P., Pozza, F., Pletcher, S.D., Gendron, C.M., Longo, V.D., 2001. Regulation of longevity and stress resistance by Sch 9 in yeast. Science 292, 288–290.

Fernandez, R., Tabarini, D., Azpiazu, N., Frasch, M., Schlessinger, J., 1995. The *Drosophila* insulin receptor homolog: a gene essential for embryonic development encodes two receptor isoforms with different signaling potential. EMBO J. 14, 3373–3384.

Fu, Y., Sander, J.D., Reyon, D., Cascio, V.M., Joung, J.K., 2014. Improving CRISPR-Cas nuclease specificity using truncated guide RNAs. Nat. Biotechnol. 32, 279–284.

Gaj, T., Staahl, B.T., Rodrigues, G.M., Limsirichai, P., Ekman, F.K., Doudna, J.A., Schaffer, D.V., 2017. Targeted gene knock-in by homology-directed genome editing using Cas9 ribonucleoprotein and AAV donor delivery. Nucleic Acids Res. 45 e98-e98.

Gantz, V.M., Bier, E.J.S., 2015. The mutagenic chain reaction: a method for converting heterozygous to homozygous mutations. Science 348, 442–444.

Gantz, V.M., Jasinskiene, N., Tatarenkova, O., Fazekas, A., Macias, V.M., Bier, E., James, A.A., 2015. Highly efficient Cas9-mediated gene drive for population modification of the malaria vector mosquito *Anopheles stephensi*. Proc. Natl. Acad. Sci. U.S.A. 112, E6736–E6743.

Hammond, A., Galizi, R., Kyrou, K., Simoni, A., Siniscalchi, C., Katsanos, D., Gribble, M., Baker, D., Marois, E., Russell, S., 2016. A CRISPR-Cas9 gene drive system targeting female reproduction in the malaria mosquito vector *Anopheles gambiae*. Nature 34, 78–83.

Hansen, M., Taubert, S., Crawford, D., Libina, N., Lee, S.J., Kenyon, C., 2007. Lifespan extension by conditions that inhibit translation in *Caenorhabditis elegans*. Aging Cell 6, 95–110.

Hietakangas, V., Cohen, S.M., 2009. Regulation of tissue growth through nutrient sensing. Annu. Rev. Genet. 43, 389–410.

Holzenberger, M., Dupont, J., Ducos, B., Leneuve, P., Géloën, A., Even, P.C., Cervera, P., Le Bouc, Y., 2003. IGF-1 receptor regulates lifespan and resistance to oxidative stress in mice. Nature 421, 182–187.

Hsu, H.J., Drummond-Barbosa, D., 2009. Insulin levels control female germline stem cell maintenance via the niche in *Drosophila*. Proc. Natl. Acad. Sci. U.S.A. 106, 1117–1121.

Jinek, M., East, A., Cheng, A., Lin, S., Ma, E., Doudna, J., 2013. RNA-programmed genome editing in human cells. Elife 2, e00471.

Kapahi, P., Zid, B.M., Harper, T., Koslover, D., Sapin, V., Benzer, S., 2004. Regulation of lifespan in *Drosophila* by modulation of genes in the TOR signaling pathway. Curr. Biol. 14, 885–890.

Kenyon, C., Chang, J., Gensch, E., Rudner, A., Tabtiang, R., 1993. A *C. elegans* mutant that lives twice as long as wild type. Nature 366, 461–464.

Kenyon, C.J., 2010. The genetics of ageing. Nature 464, 504–512.

Kim, S., Kim, D., Cho, S.W., Kim, J., Kim, J.-S., 2014. Highly efficient RNA-guided genome editing in human cells via delivery of purified Cas9 ribonucleoproteins. Genome Res. 24, 1012–1019.

Kistler, K.E., Vosshall, L.B., Matthews, B.J., 2015. Genome engineering with CRISPR-Cas9 in the mosquito *Aedes aegypti*. Cell Rep. 11, 51–60.

Kondo, S., Ueda, R.J.G., 2013. Highly improved gene targeting by germline-specific Cas9 expression in *Drosophila*. Genetics 195, 715–721.

Lin, X., Xu, Y., Jiang, J., Lavine, M., Lavine, L.C., 2018. Host quality induces phenotypic plasticity in a wing polyphenic insect. Proc. Natl. Acad. Sci. U.S.A. 115, 7563–7568.

Liu, W., Li, Y., Zhu, L., Zhu, F., Lei, C.-L., Wang, X.-P., 2016. Juvenile hormone facilitates the antagonism between adult reproduction and diapause through the methoprene-tolerant gene in the female *Colaphellus bowringi*. Insect Biochem. Mol. Biol. 74, 50–60.

Lobo, N.F., Clayton, J.R., Fraser, M.J., Kafatos, F.C., Collins, F.H., 2006. High efficiency germ-line transformation of mosquitoes. Nat. Protoc. 1, 1312–1317.

Mali, P., Yang, L., Esvelt, K.M., Aach, J., Guell, M., DiCarlo, J.E., Norville, J.E., Church, G.M., 2013. RNA-guided human genome engineering via Cas9. Science 339, 823–826.

Murillo-Maldonado, J.M., Sánchez-Chávez, G., Salgado, L.M., Salceda, R., Riesgo-Escovar, J.R., 2011. *Drosophila* insulin pathway mutants affect visual physiology and brain function besides growth, lipid, and carbohydrate metabolism. Diabetes 60, 1632–1636.

Oldham, S., Hafen, E., 2003. Insulin/IGF and target of rapamycin signaling: a TOR de force in growth control. Trends Cell. Biol. 13, 79–85.

Port, F., Chen, H.-M., Lee, T., Bullock, S.L., 2014. Optimized CRISPR/Cas tools for efficient germline and somatic genome engineering in *Drosophila*. Proc. Natl. Acad. Sci. U.S.A. 111, E2967–E2976.

Puig, O., Tjian, R., 2005. Transcriptional feedback control of insulin receptor by dFOXO/FOXO1. Genes Dev. 19, 2435–2446.

Radimerski, T., Montagne, J., Rintelen, F., Stocker, H., van der Kaay, J., Downes, C.P., Hafen, E., Thomas, G., 2002. dS6K-regulated cell growth is dPKB/dPI(3)K-independent, but requires dPDK1. Nat. Cell. Biol. 4, 251–255.

Saltiel, A.R., Kahn, C.R., 2001. Insulin signalling and the regulation of glucose and lipid metabolism. Nature 414, 799–806.

Selman, C., Lingard, S., Choudhury, A.I., Batterham, R.L., Claret, M., Clements, M., Ramadani, F., Okkenhaug, K., Schuster, E., Blanc, E., 2008. Evidence for lifespan extension and delayed age-related biomarkers in insulin receptor substrate 1 null mice. FASEB J. 22, 807–818.

Slack, C., Giannakou, M.E., Foley, A., Goss, M., Partridge, L., 2011. dFOXO-independent effects of reduced insulin-like signaling in *Drosophila*. Aging Cell 10, 735–748.

Soldatos, A.N., Metheniti, A., Mamali, I., Lambropoulou, M., Marmaras, V.J., 2003. Distinct LPS-induced signals regulate LPS uptake and morphological changes in medfly hemocytes. Insect Biochem. Mol. Biol. 33, 1075–1084.

Taniguchi, C.M., Emanuelli, B., Kahn, C.R., 2006. Critical nodes in signalling pathways: insights into insulin action. Nat. Rev. Mol. Cell Biol. 7, 85–96.

Tatar, M., Kopelman, A., Epstein, D., Tu, M.-P., Yin, C.-M., Garofalo, R., 2001. A mutant *Drosophila* insulin receptor homolog that extends life-span and impairs neuroendocrine function. Science 292, 107–110.

Umemiya-Shirafuji, R., Tanaka, T., Boldbaatar, D., Tanaka, T., Fujisaki, K., 2012. Akt is an essential player in regulating cell/organ growth at the adult stage in the hard tick Haemaphysalis longicornis. Insect Biochem. Mol. Biol. 42, 164–173.

Van Doren, M., Williamson, A.L., Lehmann, R., 1998. Regulation of zygotic gene expression in *Drosophila* primordial germ cells. Curr. Biol. 8, 243–246.

Vanhaesebroeck, B., Leevers, S.J., Ahmadi, K., Timms, J., Katso, R., Driscoll, P.C., Woscholski, R., Parker, P.J., Waterfield, M.D., 2001. Synthesis and function of 3-phosphorylated inositol lipids. Annu. Rev. Biochem. 70, 535–602.

Vermassen, E., Parys, J.B., Mauger, J.P., 2004. Subcellular distribution of the inositol 1, 4, 5-trisphosphate receptors: functional relevance and molecular determinants. Biol. Cell. 96, 3–17.

White, M.F., 1998. The IRS-Signalling System: a Network of Docking Proteins that Mediate Insulin Action, Insulin Action. Springer, pp. 3–11.

Xu, H.J., Xue, J., Lu, B., Zhang, X.C., Zhuo, J.C., He, S.-F., Ma, X.F., Jiang, Y.Q., Fan, H.W., Xu, J.Y., Ye, Y.X., Pan, P.L., Li, Q., Bao, Y.Y., Nijhout, H.F., Zhang, C.X., 2015. Two insulin receptors determine alternative wing morphs in planthoppers. Nature 519, 464–467.

Xue, W.H., Xu, N., Yuan, X.B., Chen, H.H., Zhang, J.L., Fu, S.J., Zhang, C.X., Xu, H.J., 2018. CRISPR/Cas9-mediated knockout of two eye pigmentation genes in the brown planthopper, *Nilaparvata lugens* (Hemiptera: Delphacidae). Insect Biochem. Mol. Biol. 93, 19–26.

Zhang, C.X., Brisson, J.A., Xu, H.J., 2019. Molecular mechanisms of wing polymorphism in insects. Annu. Rev. Entomol. 64, 297–314.

Zuris, J.A., Thompson, D.B., Shu, Y., Guilinger, J.P., Bessen, J.L., Hu, J.H., Maeder, M.L., Joung, J.K., Chen, Z.Y., Liu, D.R., 2015. Cationic lipid-mediated delivery of proteins enables efficient protein-based genome editing *in vitro* and *in vivo*. Nat. Biotechnol. 33, 73–80.